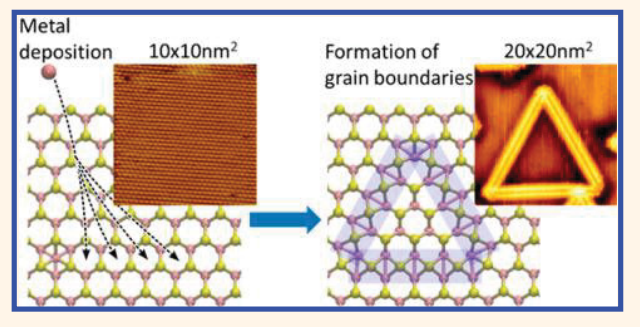
Post-Synthesis Modifications of Two-Dimensional MoSe₂ or MoTe₂ by Incorporation of Excess Metal Atoms into the Crystal Structure

Paula Mariel Coelho,[†] Hannu-Pekka Komsa,[‡] Horacio Coy Diaz,[†] Yujing Ma,[†] Arkady V. Krasheninnikov,^{§,‡} and Matthias Batzill*,[†]

Supporting Information

Downloaded via UNIV OF SOUTH FLORIDA on April 3, 2019 at 20:37:14 (UTC). See https://pubs.acs.org/sharingguidelines for options on how to legitimately share published articles.

ABSTRACT: Phase engineering has extensively been used to achieve metallization of two-dimensional (2D) semiconducting materials, as it should boost their catalytic properties or improve electrical contacts. In contrast, here we demonstrate compositional phase change by incorporation of excess metals into the crystal structure. We demonstrate post-synthesis restructuring of the semiconducting MoTe₂ or MoSe₂ host material by unexpected easy incorporation of excess Mo into their crystal planes, which causes local metallization. The amount of excess Mo can reach values as high as 10% in MoTe₂ thus creating a significantly altered material compared



to its parent structure. The incorporation mechanism is explained by density functional theory in terms of the energy difference of Mo atoms incorporated in the line phases as compared to Mo ad-clusters. Angle resolved photoemission spectroscopy reveals that the incorporated excess Mo induces band gap states up to the Fermi level causing its pinning at these electronic states. The incorporation of excess transition metals in MoTe₂ and MoSe₂ is not limited to molybdenum, but other transition metals can also diffuse into the lattice, as demonstrated experimentally by Ti deposition. The mechanism of incorporation of transition metals in MoSe2 and MoTe2 is revealed, which should help to address the challenges in synthesizing defect-free single layer materials by, for example, molecular beam epitaxy. The easy incorporation of metal atoms into the crystal also indicates that the previously assumed picture of a sharp metal/2Dmaterial interface may not be correct, and at least for MoSe₂ and MoTe₂, in-diffusion of metals from metal-contacts into the 2D material has to be considered. Most importantly though, the process of incorporation of transition metals with high concentrations into pristine 2D transition-metal dichalcogenides enables a pathway for their post-synthesis modifications and adding functionalities.

KEYWORDS: transition-metal dichalcogenides, crystal modifications, metal contacts, inversion domains, grain boundaries, metal interstitials

tomic structure engineering of two-dimensional (2D) materials by introducing dopants,^{1,2} point defects,³ inducing phase transitions,^{4–7} alloying,⁸ creating innterfaces,^{9,10} or boundaries between grains^{11–17} enables plane interfaces,9 addition of functionalities to these materials. As for the latter, mirror twin boundaries (MTBs) between grains rotated by 60° have been found in Mo-based transition-metal dichalcogenides (TMDs) and identified as Mo-rich one-dimensional (1D) structures. 11,12,16-19 These structural modifications can be prominent in monolayers of MoSe2 and MoTe2 grown by molecular beam epitaxy. 20,21 Interestingly, it has been shown by density functional theory (DFT) calculations 11,22 and experimentally observed^{23,24} that MTBs exhibit metallic electronic bands with finite dispersion. Because of the confinement of the metallic states, they show intriguing 1D quantum liquid behavior described by the Tomonaga-Luttinger liquid theory and are the first 1D metal for which spin-charge separation has

Received: February 28, 2018 Accepted: March 29, 2018 Published: April 9, 2018

[†]Department of Physics, University of South Florida, Tampa, Florida 33620, United States

[‡]Department of Applied Physics, Aalto University, 00076 Aalto, Finland

[§]Institute of Ion Beam Physics and Materials Research, Helmholtz-Zentrum Dresden-Rossendorf, 01328 Dresden, Germany

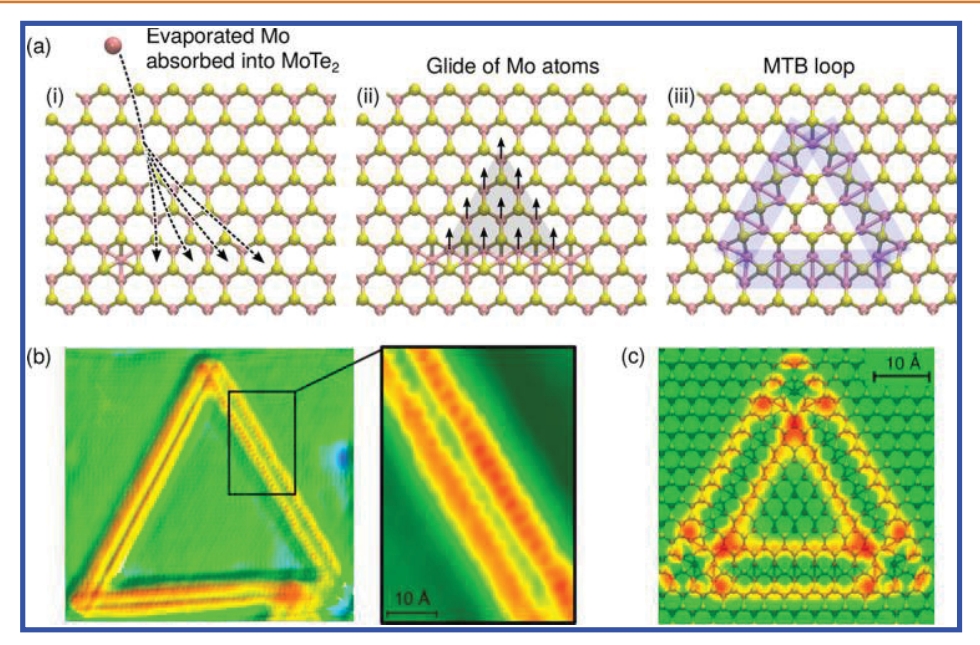


Figure 1. Schematic illustration of the formation of an ID surrounded by an MTB loop by incorporation of excess Mo into the Mochalcogenide lattice and its experimental verification in STM. A schematic model for the formation of an ID is shown in (a). Mo incorporation into the pristine lattice (i) and subsequent translation of a portion of the Mo sublattice (ii) causes the formation of an ID surrounded by a MTB loop (iii). Such MTB loops can be observed by STM shown in (b) (V_{bias} : -1.1 V; I_{t} : 0.7 nA) for a MTB loop structure with about 50 added Mo atoms in MoSe₂. The experimental STM image of the double-row structure is reproduced well in Tersoff—Hamann simulated STM images shown in (c). Note that the simulated system is much smaller than the experimental one in panel (b).

been experimentally confirmed. Also, as expected for 1D metals, a Peierls' metal-to-insulator instability has been observed with transition temperature of \sim 230 K for MoSe₂. 23,24

2D materials consist of surface only, and consequently their stoichiometry and morphology can be modified more easily as compared to bulk systems, ²⁵ and this potentially enables tuning of their properties over a wider range, adding to the functionalities of 2D materials. Post-synthesis phase change of MoS₂ or MoTe₂ from the semiconducting 2H to metallic 1T or 1T' structures by charge doping or thermal processing has been suggested to modify their catalytic properties 26,27 as well as an approach for making better electrical contacts to 2D materials. 6,28-30 Long-term phase stability and/or stability at the interfaces as well as processing conditions are, however, potential limitations of such phase engineering methods. Thus, crystal engineering by the introduction of dense MTB networks by locally controlled post-synthesis stoichiometry modifications could be an alternative approach for the introduction of metal contacts in 2D materials and to tune chemical functionalities. So far, the mechanism of formation of MTB networks is not understood, and consequently no process of their controlled formation has been demonstrated. Here we show that incorporation of excess Mo into MoSe2 or MoTe 2 lattice, but not MoS₂, results in the self-formation of MTB networks. We also demonstrate that the incorporation of excess metals into MoTe₂ is not limited to Mo: other transition metals, namely Ti, are also readily incorporated in this 2D material at interstitial sites.

RESULTS AND DISCUSSION

In previous studies of mono- to few-layer MoSe₂ or MoTe₂ growth by molecular beam epitaxy (MBE), the formation of MTB networks was observed by various groups. ^{11,16,20,23,24,31} Although the structure and composition of these MTBs were

determined by transmission electron microscopy, the origin and mechanism for their formation remained unresolved. Contrary to other types of grain boundaries that require rotation of neighboring grains, MTBs can be viewed as 1D compositional modifications of the TMD lattice. The relationship between the atomic structure of a pristine TMD sheet and that with an inversion domain (ID) and the associated MTB is shown in Figure 1a. Schematically, extra Mo atoms form a line, then a part of the Mo sublattice is translated relative to the rest of the system, thus creating an ID without the need of a lattice rotation. This simple model suggests that MTB triangular loops and eventually dense networks of MTBS may be formed by incorporation of excess Mo into the crystal structure. This begs the question if the observed MTB networks in MBE grown samples are formed during growth, for instance by coalescence of twin grains, or if such networks can form "post-growth" by incorporation of excess Mo (note that elemental Mo is constantly supplied during MBE- growth) into the already grown MoSe₂ or MoTe₂ film. Here we demonstrate that the latter is the case by facilitating MTB formation by deposition of Mo onto a pristine single crystal surface, that is, without any growth process of MoSe₂ or MoTe₂. This astonishing result is confirmed by DFT calculations and has several important implications, specifically it allows for controlled post-synthesis crystal modifications.

Formation of MTB Networks by Incorporation of Excess Mo into the Lattice. To address the question if layered materials can be modified with MTB networks by incorporation of excess Mo, we start with single crystals of MoS₂, MoSe₂, or MoTe₂ and deposit elemental Mo from a high purity Mo rod with an e-beam evaporator under ultrahigh vacuum. Before deposition, the surfaces show only isolated defects that are well-documented in the literature to occur on single crystals.³² Atomic resolution STM images reveal well-

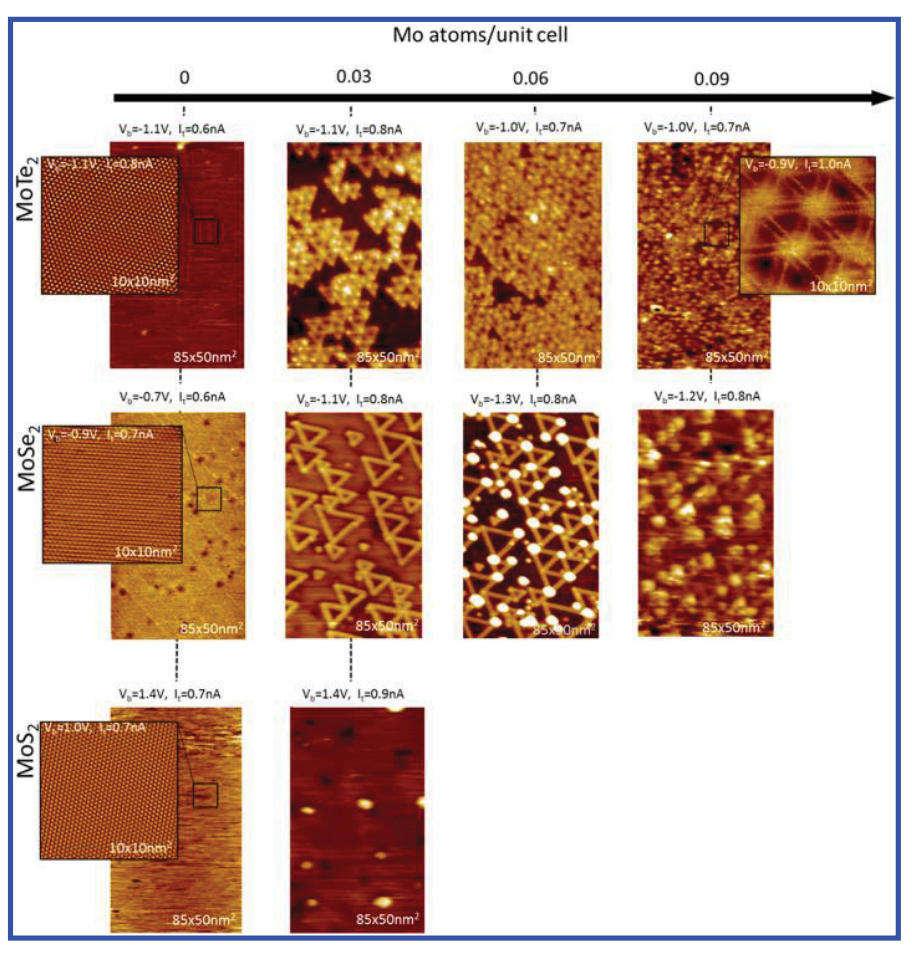


Figure 2. STM images for sequential deposition of Mo at 350 °C on the three different Mo-dichalcogenides substrates. The axis is based on the normalized number of Mo atoms absorbed within the unit cell of MoTe₂.

ordered crystalline surfaces as shown in Figure 2. The figure also presents STM images for sequential deposition of Mo on these three different Mo-dichalcogenide single crystal surfaces at 350 °C. With increasing Mo deposition, the three surfaces evolve differently. On both MoTe₂ and MoSe₂, triangular MTB loops form, while on MoS2 only formation of metal clusters is observed. In high-resolution filled state images, the triangular defects in MoSe₂ and MoTe₂ appear as two bright parallel lines. The STM images of such structures are illustrated by the example of MoSe₂ in Figure 1b. To demonstrate that these two parallel lines correspond to MTBs, we performed Tersoff-Hamann simulations of the STM images of an ID separated by MTBs shown in Figure 1c. These simulations reveal the same double row structure indicating that in filled state images, the chalcogen atoms adjacent to the actual MTBs are imaged "bright". The excellent match between the experimental STM data and the simulated ones for MTBs confirms that the line structures formed by Mo depositions in MoSe₂ and MoTe₂ are indeed MTB loops. This is also consistent with previously reported STM images of MTBs in MBE grown monolayers.^{20,21,23,24} In our experiment, deposition of Mo on MoSe₂ eventually results in the formation of Mo ad-clusters. The transition from formation of triangular MTB loops to nucleation of Mo clusters occurs at ~0.05 ML of excess Mo for the growth conditions in this experiment. The Mo clusters preferentially nucleate at the corners of the triangular MTB loops, indicating that these are high-energy sites for metal

nucleation. On MoTe₂, on the other hand, the density of the MTB network keeps increasing beyond the saturation coverage observed for MoSe₂. We observe that 15–20% of a ML of excess Mo can be incorporated into MoTe₂. Further deposition eventually also results in the formation of Mo clusters at the surface. The higher Mo concentration in the MTBs implies that for MoTe₂ and for MoSe₂, but not for MoS₂, Mo atoms can readily diffuse into the crystal plane of the TMD and self-organize into ordered 1D crystal structures embedded in the TMD lattice.

MTBs can also be obtained by room-temperature (RT) deposition of Mo and subsequent annealing. Deposition of a small amount of Mo (1 excess-Mo/200 unit cells) at RT forms point like defects in MoTe₂ as shown in Figure 3a. The inset in Figure 3a shows high-resolution images that indicate that these point defects appear as three short bright lines in filled state images. Only one kind of defect configuration is observed after RT deposition. The contrast observed in STM suggests that these are single Mo interstitial sites. Like demonstrated above for the MTBs, it is the chalcogen atoms adjacent to the defect site that appear bright in STM. Figure 4 shows a detailed STM image of a single protrusion. It appears that the center is imaged dark if filled states are probed. This dark center is surrounded by three bright protrusions that form almost a complete triangle. Key features of this experimental image are reproduced by Tersoff-Hamann STM simulations of a Mo interstitial as shown in Figure 4c,d. The simulations also show a

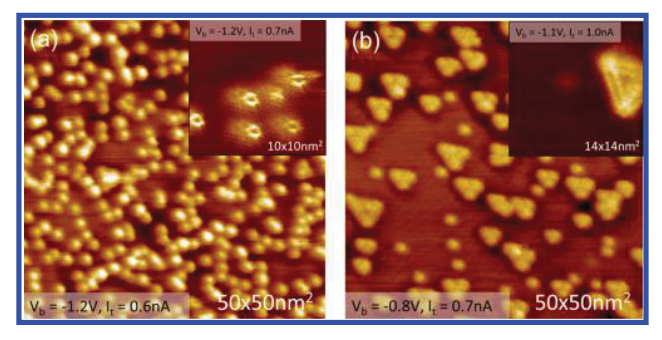


Figure 3. STM studies of MoTe $_2$ surfaces with Mo deposited at RT and subsequent annealing. (a) Large-scale STM images of MoTe $_2$ after Mo deposition at RT. The inset shows the structure of individual Mo-induced point defects (likely Mo interstitials). (b) Large-scale STM images of MoTe $_2$ after annealing at 250 °C. Annealing at such temperature converts the point defect into MTB loops clearly resolved in the inset.

dark center surrounded by three bright spots. In the experimental STM images, however, the bright regions are more extended forming a triangular shape. To obtain agreement with the experiment, one has to assume that the three bright spots in the simulated STM image are not the corners of a triangular feature but rather the sides of the triangle in the measurements. The agreement between the extension of the defect in STM and those predicted for an interstitial in the

simulated STM image is best seen in the lattice superimposed. Importantly, while after RT deposition almost exclusively individual interstitial sites are detected, these interstitials appear to agglomerate into triangular MTB loops, as shown in Figure 3b, after annealing of the sample to 250 °C. From the initial density of bright protrusions in the STM image after RT deposition and the length of line defects after annealing, it is apparent that each initial protrusion converts into ~1 nm of MTB loop length. This conversion is consistent with the schematic in Figure 1, provided that every initial protrusion corresponded to one excess Mo atom. This further verifies our assignment of the protrusions to a single Mo interstitial. Importantly, the formation of MTBs by annealing to 250 °C suggests sufficient mobility of the Mo interstitials to aggregate into MTBs.

The experiments demonstrate that excess Mo modifies the lattice structure of MoSe₂ and MoTe₂ with metallic 1D-structural motifs. For MoS₂, this process does not occur. To gain insight on the energetics of this process and potential pathways for the formation of extended MTBs, we performed detailed DFT simulations.

Comparison of Formation Energies of Excess Mo in Ad- or Interstitial Sites. First, we compare the formation energies of Mo adatoms with those of two kinds of Mo interstitials in the Mo-dichalcogenide lattice, as shown in Figure 5a. Formation energy for the system containing n_{Mo} additional Mo atoms is defined as $E_f = E(\text{defect}) - E(\text{pristine}) - n_{\text{Mo}}\mu_{\text{Mo}}$,

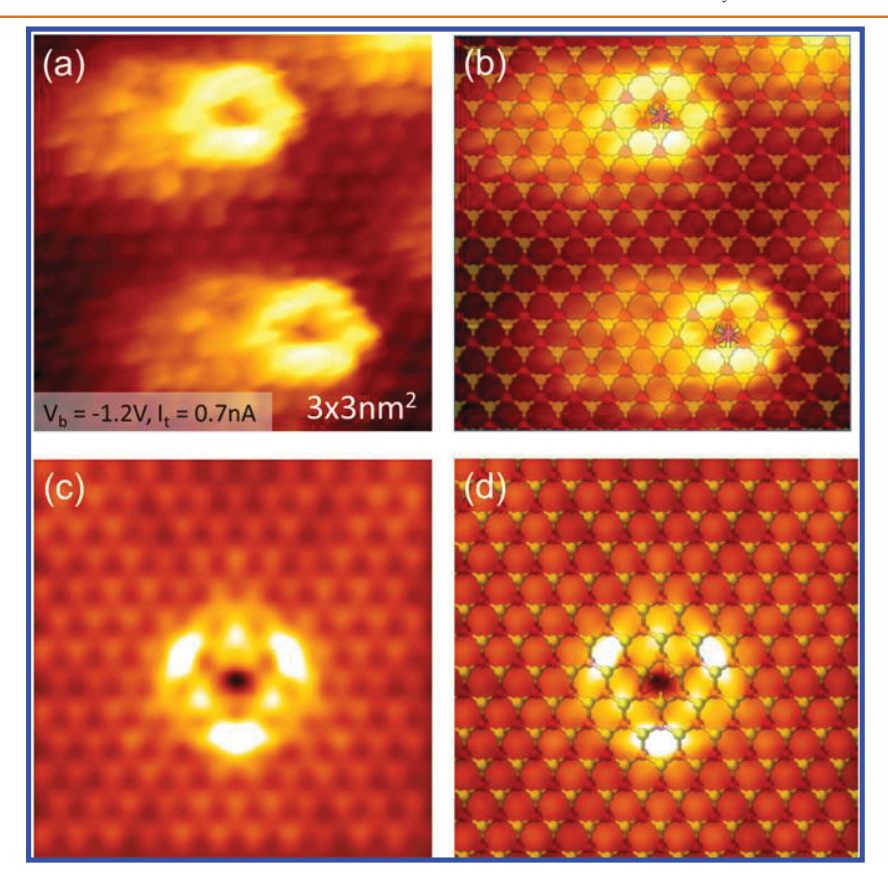


Figure 4. STM of single Mo interstitial in $MoTe_2$. A filled-state STM image ($V_{bias} = -1.2 \text{ V}$) is shown in (a) with a ball-and-stick model overlaid in (b). The dark center of the defect is close to the interstitial site using the atomic corrugation of the surrounding structure as indicators for the Te sublattice. Simulated STM images are shown in (c) and in (d) with the superimposed lattice. The important point is that the actual interstitial site is imaged as a depression and the surrounding is imaged brighter in a triangular configuration, in agreement with the experiment.

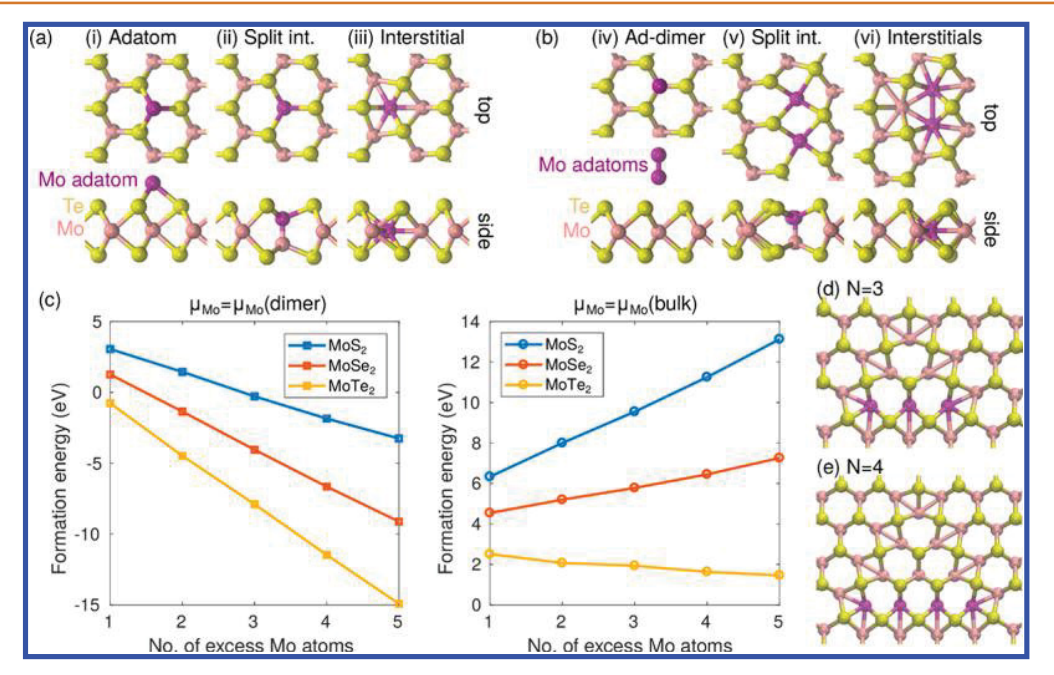


Figure 5. Configurations and formation energies of excess Mo incorporated into Mo-dichalcogenides. (a) Atomic configurations for defects involving a single additional Mo atom in 2D TMDs: (i) adatom, (ii) interstitial, and (iii) split interstitial. (b) Atomic configurations for defects involving two additional Mo atoms: (iv) ad-dimer, (v) a pair of split interstitials in nearest neighbor (NN) sites, and (vi) a pair of NN interstitials. (c) Energy difference between the system with inversion domain and the pristine TMD sheet with a corresponding number of Mo atoms either in the dimer or bulk crystal. (d,e) Atomic structures of inversion domains with three and four extra Mo atoms.

Table 1. Formation Energies for All Configurations Shown in Figure 4^a

		formation energies (eV) for single excess Mo atom (Figure 5a) $\mu_{\rm Mo} = \mu_{\rm Mo}$ (atom)			formation energies (eV) for two excess Mo atoms (Figure 5b) $\mu_{\rm Mo}=\mu_{\rm Mo}$ (dimer)		
	a (Å)	adatom	split int.	interst.	addimer	split-pair	int-pair
MoS_2	3.18	-1.48	-2.51	0.14	-0.74	0.91	1.45
$MoSe_2$	3.32	-1.05	-2.26	-1.72	-0.46	1.13	-1.35
$MoTe_2$	3.55	-1.08	-2.15	-3.85	-0.60	0.01	-4.48

"Calculated lattice constants are also shown. Bold text highlights the most stable configuration. For defects with a single Mo atom, we choose a reference corresponding to Mo atom in vacuum. For defects with two Mo atoms, we choose a reference with a Mo dimer in vacuum.

where E(defect) is the total energy of the system with extra Mo atoms, E(pristine) is the energy of the pristine system, and Mo chemical potential μ_{Mo} is chosen depending on the deposition stage. We considered a split interstitial site, that is, the occupation of the regular Mo site with two Mo atoms and a regular interstitial site in the center of the hexagonal structure. For all Mo-dichalcogenides, formation of interstitials or split interstitials is favored over adatoms, as evident from Table 1. MoTe₂ prefers the regular interstitial site, while MoSe₂ and MoS₂ prefer split interstitial sites. Thus, single Mo atoms should always have a tendency to be incorporated into the lattice. Only a modest potential kinetic barrier has to be overcome for the excess Mo to go from an adatom site to an interstitial site, which we have estimated to be 0.6, 0.2, and 0.4 eV for MoS₂, MoSe₂, and MoTe₂, respectively (see Supporting Information). With increasing Mo deposition, the formation energy of interstitials or pairs of interstitials should, however, be compared to the formation energy of adsorbed dimers or Mo clusters rather than individual adatoms. The energy difference determines if the interstitials are still energetically favored over adsorbed Mo clusters, that is, if it remains energetically favorable for two (split) interstitials to remain in the lattice or adsorbed dimers become favored. Comparison of the formation energies, shown in Table 1, reveals that only for MoSe₂ and MoTe₂ the interstitial site is favored over adsorbed Mo dimers, while for MoS₂, adsorbed Mo dimers are preferable. Consequently, one would expect that two Mo split interstitials combine to an adsorbed Mo dimer for MoS₂. Incorporation of three or more excess Mo atoms allows the formation of MTBs, as indicated in Figure 5d,e.

Formation of MTBs by Agglomeration of Mo Interstitials. With increasing the number of excess Mo atoms or correspondingly the lengths of the MTB loop, the formation energy of the MTB is defined as a difference between the total energy of the system with the MTB and pristine system with Mo dimers on its surface decreases for all TMDs, (Figure 5c), indicating that the formation of MTBs is energetically favorable over dimer formation. As further Mo is deposited on the surface, the proper energy reference for the MTBs could correspond to larger Mo clusters. However, since this leads to exponentially increasing computational complexity and the multiple structures are likely to coexist, we only consider the limiting case of bulk Mo. In this case, formation energies are positive, but the energy difference for MoTe₂ is much lower than for other TMDs, and it is going down with the size of IDs. As the chemical potential of Mo atoms in clusters should be between those in the dimer and bulk crystal, one can expect that IDs and MTBs should easily appear in

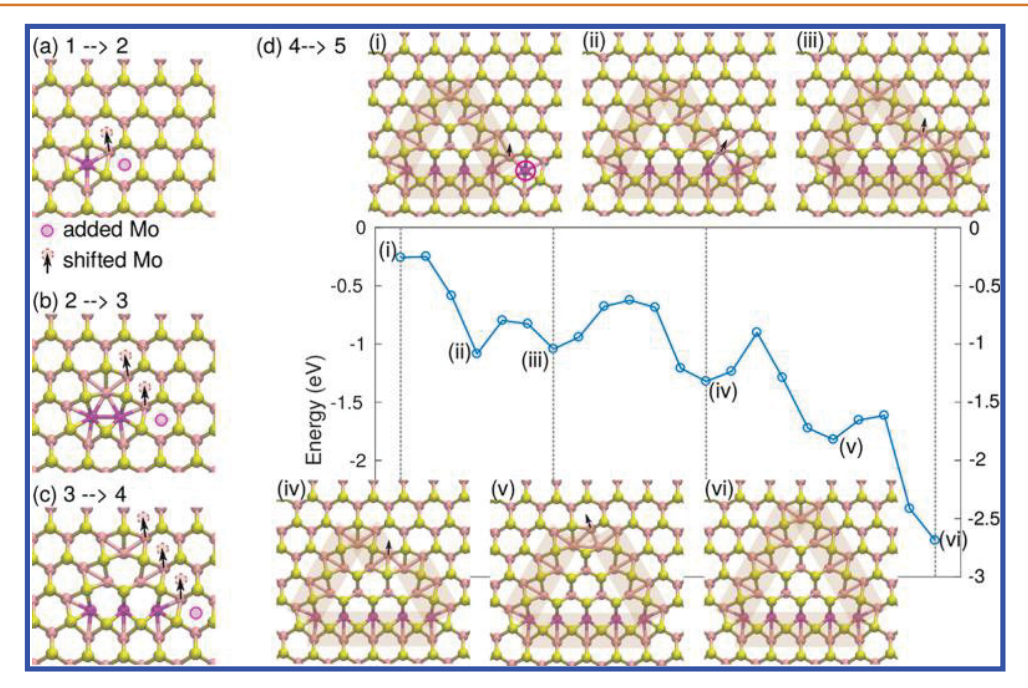


Figure 6. Illustration and energy barriers for the growth of a MTB loop by addition of an extra excess Mo atom. (a-d) Illustration of the atomic mechanism for the enlargement of the MTB loop (from size N to N+1) by addition of excess Mo (magenta atoms). The magenta circle denotes the position of the next added Mo and the black arrow the subsequent shift of the neighboring Mo atom(s) with the final position shown by brown circles. (d) Atomic configurations and the corresponding energy landscape for the transformation from N=4 to N=5, showing overall decrease in energy. All barriers between local energy minima are within 0.2–0.5 eV. Zero energy corresponds to MTB loop of size N=4 and isolated Mo interstitial, indicating that the corner site is more favorable.

MoTe₂ and hardly in MoS₂, while MoSe₂ is an intermediate case, as observed in the experiments.

The decrease in MTB formation energy with increasing ID size implies that it is energetically favorable for an ID to grow in size by incorporating excess Mo atoms. In our experiments we utilize a very low Mo deposition rate that effectively adds one Mo atom at a time, and this facilitates the MTB growth. The observed higher density of MTBs and thus smaller IDs in MoTe₂ as compared to MoSe₂ may be associated with the lower formation energies in MoTe2, which causes higher nucleation rates. Besides, in MoSe₂ it is easier for an isolated Mo split interstitial to "resurface" and attach to a growing MTB through surface diffusion than in MoTe₂. This may also contribute to the larger MTB loops in MoSe₂, for example, the one in Figure 1b, which contains ~50 excess Mo atoms. In MoSe₂ the growth of the MTB loops seems only limited when the growing MTB meets neighboring MTBs, at which point Mo-cluster formation sets in, because the MTB cannot grow any further.

For the growth of MTBs to happen, the energy barriers for adding more Mo atoms to an existing MTB must be low. Thus, to understand the process of MTB growth, we evaluated kinetic barriers for the diffusion of interstitials and the conversion of interstitials into MTBs. Experimentally we demonstrated that annealing to $\sim \! 500$ K is sufficient for the formation of MTBs, suggesting a modest barrier for diffusion of Mo interstitials and the formation of MTB loops. We use DFT simulations to calculate the barriers for diffusion of interstitials and (split) interstitials in MoTe2 and MoSe2. From these barriers we estimated that Mo interstitials are very mobile in MoTe2 and can diffuse at 200 K, while in MoSe2 split interstitials encounter significantly larger barriers but can diffuse at 600 K. The considered pathways of diffusion and their barriers are

illustrated in Figures S1 and S2. A proposed atomic mechanism for the formation of MTBs by sequential incorporation of excess Mo into the MoTe₂ lattice and their energy gains are illustrated in Figure 6. By adding a Mo atom near the corner of the ID and shifting the neighboring Mo atoms of the MTB to the adjacent interstitial site, the MTB effectively moves by one lattice constant. Figure 6d also shows the energy landscape for the growth from ID size 4 to size 5. The energy decreases with the highest barrier between local energy minima are only about 0.5 eV, thus demonstrating that such process can readily occur. The initial structure is justified by noting that the energy for adding Mo interstitial near the corner of the MTB loop is favored by 0.25 eV over interstitial being far from it.

Defect-Induced Band Gap States by MTB Network. The easy incorporation of excess Mo into the lattice of MoSe₂ or MoTe₂ implies the formation of additional electronic states due to the excess Mo-induced MTB networks. It has been previously shown for MTBs in MoSe2 that they exhibit metallic properties and undergo a Peierls transition as expected for 1D metals. A high density of states in the band gap of the semiconducting MoSe₂ or MoTe₂ is likely to induce pinning of the Fermi-level at these gap-states, not different from the Fermi-level pinning observed at reconstructed semiconductor surfaces or at metal-induced gap states in metal/semiconductor interfaces. Knowledge of the Fermi-level position in MTB modified MoSe₂ or MoTe₂ thus is crucial if these modifications are going to be used to fabricate controlled metal contacts. To gain insight in the electronic structure and defect-induced electronic states in the surface modified by MTBs, we performed ARPES studies. Figure 7 shows band dispersion along the Γ -K direction of the BZ for single crystal MoSe₂ and MoTe₂. Note that for single crystals the valence band maximum is at the Γ -point. Both single crystals are n-doped, which is the

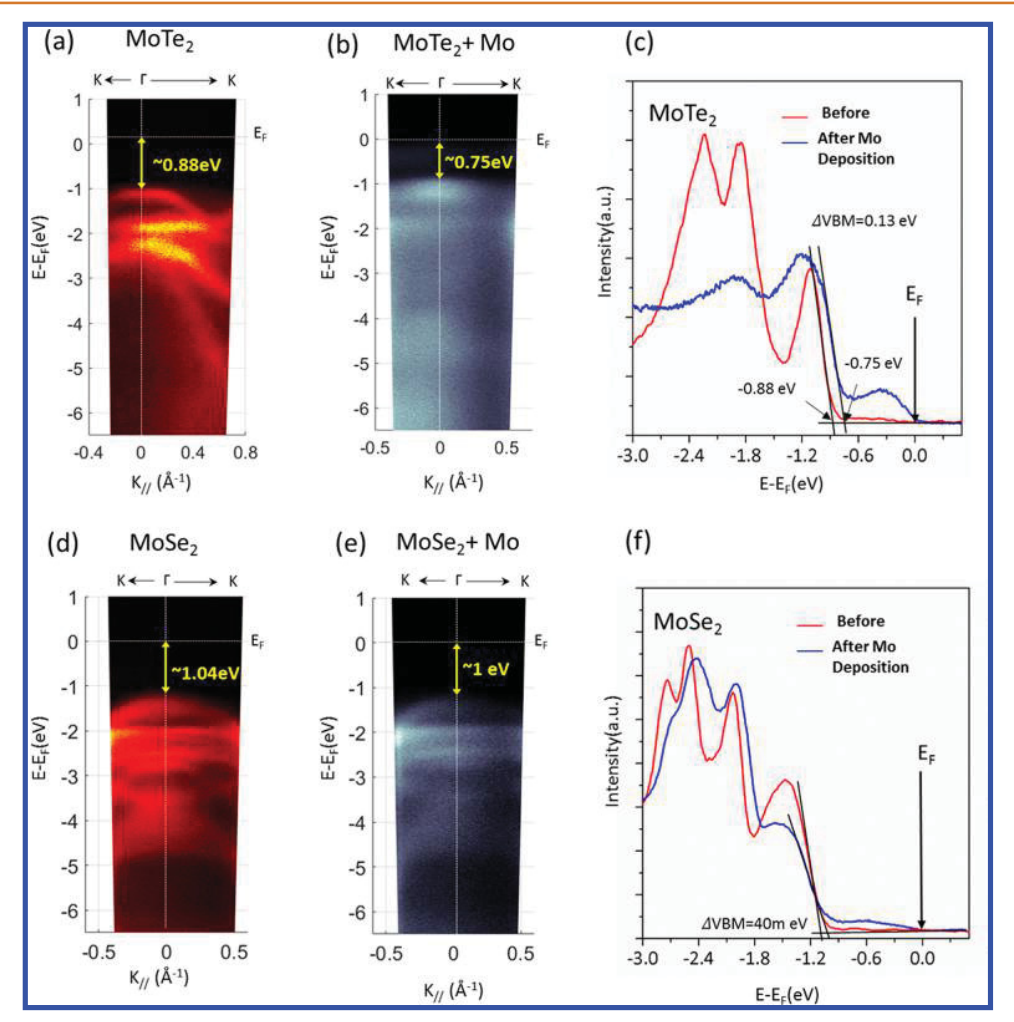


Figure 7. ARPES studies of $MoTe_2$ and $MoSe_2$ single crystal surface before and after MTB formation in the vicinity of the Γ -point. He-II ARPES spectra of the $MoTe_2$ single crystal before and after Mo deposition at 350 °C are shown in (a) and (b), respectively. The comparison of energy distribution curves of the electron densities at the Γ -point, before and after Mo deposition, is shown in (c). He-II ARPES spectra of the $MoSe_2$ single crystal before and after Mo deposition at 350 °C are shown in (d) and (e), respectively. The comparison of energy distribution curves of the electron densities at the Γ -point, before and after Mo deposition, is shown in (f). The lower concentration of MTBs in $MoSe_2$ compared to $MoTe_2$ gives rise to the weaker intensity close to the Fermi-level for the $MoSe_2$ sample.

natural doping of Mo-dichalcogenides and is likely originating from doping by intrinsic defects. After formation of MTBs by deposition of Mo at 350 °C, the valence band maximum (VBM) at the Γ -point is shifting closer to the Fermi-level, that is, it becomes slightly less n-doped. This shift is due to the pinning of the Fermi-level at MTB-induced states. These states are better seen in energy distribution curves (EDCs) measured at the Γ -point and shown in Figure 7c,f for MoTe₂ and MoSe₂, respectively. The EDCs clearly indicate the band gap states extending up to the Fermi-level and shift of the VBM of 130 and 40 meV for MoTe₂ and MoSe₂, respectively. This means that the VBM at the Γ -point occurs at 0.75 and 1.0 eV for MoTe₂ and MoSe₂ for surfaces modified with MTBs. These latter values for the VBM is expected to be independent of the initial doping of the sample since the Fermi-level position in the MTB modified material is pinned at the defect states. We also performed measurements at the K-point, because the electronic states at the K-point are less influenced by formation of IDs in MTB networks. 33 These measurements gave similar results and can be found in Figure S4.

Titanium Incorporation into MoSe₂ and MoTe₂ **Lattices.** The above discussion of the controlled formation of MTBs by Mo deposition shows that this is an approach to locally metallize these materials with defined Fermi-level position with respect to the VBM of the semiconductor parent material. The apparently easy incorporation of Mo into the lattices of MoSe₂ and MoTe₂ also raises the question if other transition metals may also diffuse into the 2D lattice rather than remaining at the surface. If this was the case, then, for example, deposition of metal contacts onto TMDs may be inadvertently already modified by transition metals in interstitial sites or by MTB networks underneath the metal contact patches. This would be a very different scenario to the general simplified view of sharp metal/2D-material interfaces with chemical interactions of the metal with only the topmost chalcogen atoms of the TMD.³⁴ To address this important issue for metal/TMD interfaces, we study titanium deposition in the ultralow coverage limit with the goal to investigate if Ti remains at the surface or occupies interstitial sites. Ti and its alloys are prototypical materials used for making well-adhering metal contacts on 2D materials, and thus its diffusion into the 2D

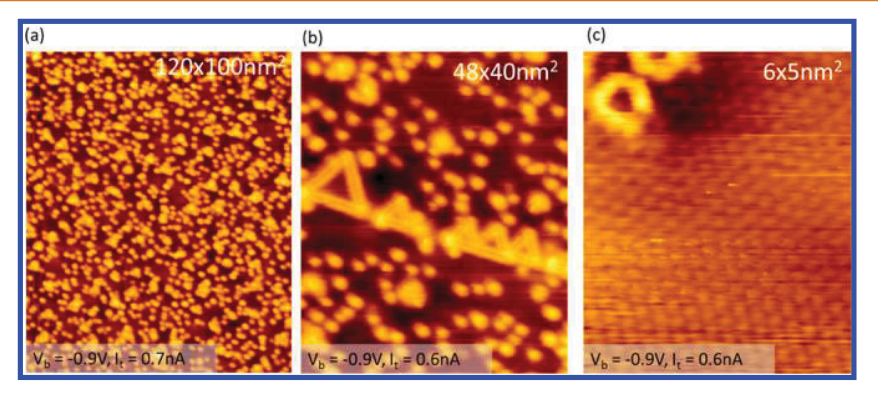


Figure 8. STM of 0.3% of a titanium ML deposited on MoTe₂ at 350 °C. (a) Large-scale image showing single protrusions together with some small triangular MTBs. (b) Some larger triangular MTB loops are occasionally observed that appear to be aligned, thus suggesting that some pre-existing line defect in the substrate may assist their formation. (c) Zoom-in on bright protrusions shows a similar ring structure as has been observed for single Mo-interstitial sites, suggesting that every protrusion is due to a Ti interstitial.

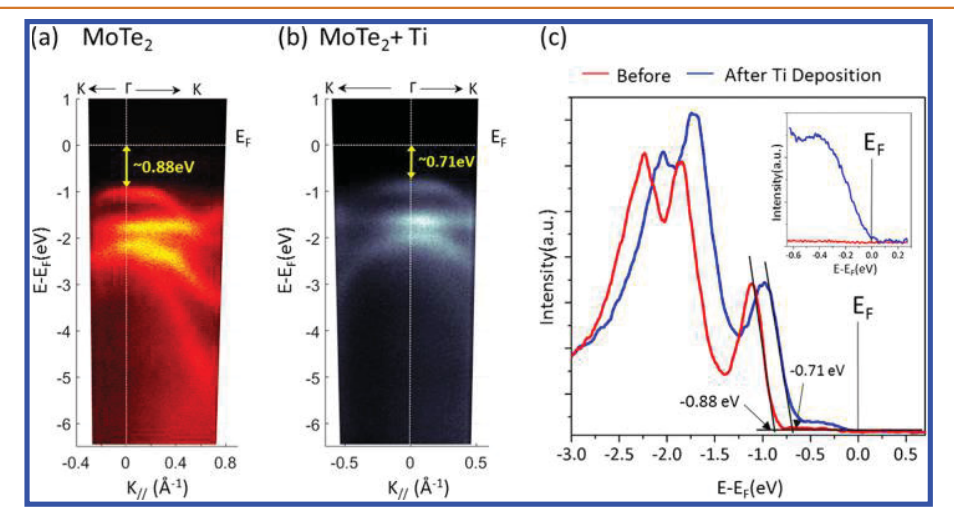


Figure 9. ARPES studies of MoTe₂ and MoTe₂ + Ti. He-II ARPES spectra of the MoTe₂ single crystal before and after Ti deposition at 350 $^{\circ}$ C are shown in (a) and (b) respectively. (c) Comparison of energy distribution curves at the Γ -point, before and after Ti deposition. The inset shows the electron densities close to the Fermi level.

material would suggest a drastic change in the metal/2D-material interface compared to previous models.

Figure 8 shows the surface of MoTe₂ after deposition of \sim 0.3% of a ML of Ti with the sample at 350 °C (where 1 ML is defined as the number of Mo atoms in the MoTe₂ monolayer, i.e., 1 ML corresponds to one Ti atom per MoTe₂ unit cell). We observe mostly small protrusions and only a few triangular MTB loops. Occasionally, we observe large MTB loops with several of them being aligned, as shown in Figure 8b. Zooming in on the small protrusions, presented in Figure 8c, we identify the same "ring" structure that we associated with single interstitial atoms for Mo deposition. This suggests that the protrusions are also due to transition-metal interstitials, but in this case they are the consequence of Ti atoms at the interstitial sites in MoTe2, and thus different transition-metal interstitials appear to give similar contrast in STM images. It is interesting to point out that for Mo deposition, we observe many more MTB loops for the same deposition temperature and similar coverage than for Ti deposition. This implies that Ti interstitials are less mobile than Mo interstitials or prefer to stay as single interstitials rather than to agglomerate. The observation of multiple large triangular MTB loops along a line may suggest that these form along pre-existing defects in the crystal along which the diffusion may be enhanced. Preferred

formation of Ti interstitials compared to Ti- adatoms or Ti in split-interstitial sites is also confirmed by DFT simulations. Our calculations indicate that the formation energy for Ti interstitials is -4.93 eV and is energetically favored by 2.59 eV compared to a Ti adatom. It is also interesting to note that formation energy for Ti interstitials is favored as compared to Mo interstitials (-3.85 eV; see Table 1), further stressing the strong preference for Ti to form interstitials in MoTe₂. This large formation energy of Ti in the interstitial site may also contribute to its stability and larger barriers for diffusion. In addition, diffusion should proceed *via* a site exchange of the Ti interstitial with a Mo lattice atom. We calculate that the configuration of such a site exchange is energetically disfavored by 0.2 eV. While this is a relative small energy, it will add to the barrier of diffusion for Ti.

Finally, ARPES measurements of Ti-modified MoTe $_2$ are shown in Figure 9. Similar to the case of excess Mo, band gap states are observed that pin the Fermi level, as can be seen from the EDC at the Γ -point shown in Figure 9c. The VBM is measured to be at 0.71 eV below the Fermi level at the Γ -point for the Ti-modified surface. This is slightly closer to the Fermi level than for Mo-modified MoTe $_2$ where the VBM was found at 0.75 eV. This indicates that the Fermi-level pinning occurs at a slightly different energy in the band gap for Ti-modified

MoTe₂ than for MoTe₂ modified by excess Mo. This shows that for some TMDs, the incorporation of excess transition metals into the lattice has to be taken into account when modeling the metal/TMD interface. We stress that the intermixing of the metal with the TMD is not universal. One possible explanation for the easier incorporation of excess metals in MoTe₂ or MoSe₂ compared to MoS₂ is that the larger unit cells of the former enables the incorporation of excess transition metals in interstitial sites and their subsequent restructuring into 1D crystal modifications.

CONCLUSIONS

In conclusion, we have shown that the morphology of MoTe₂ and to a lesser extent MoSe₂ can be altered by incorporation of excess Mo. The excess Mo organizes itself into metallic 1D structures, and their dense networks represent a Mo-rich 2D phase of these materials. The easy incorporation of excess Mo in these materials explains the mechanism responsible for the formation of such MTB networks in MBE grown monolayers of MoSe₂ and MoTe₂. 16,20,21 Our observations also imply that some of the simple models of metal/TMD interfaces that suggest that the ad-metal only interacts with the topmost chalcogen atoms may need to be reconsidered for certain metal/TMD interfaces. Specifically, our studies show that at least for Ti or Mo interfaces with MoTe₂ or MoSe₂ the system can be far more complex and metal in-diffusion and crystal modifications may occur. Finally, we want to point out that the understanding of excess metal-induced crystal modifications opens opportunities for further functionalization of TMDs, which may be particularly important for chemical transformation reactions over TMD catalysts.

METHODS

Sample Preparation. Commercial TMD single crystals (Graphene HQ) were cleaved in air by scotch tape and immediately introduced into the vacuum chamber. The TMDs were outgassed for 2 h at 250 °C. Atomic Mo or Ti was deposited by sublimation of Mo or Ti from a 2 mm high-purity metal rod. The rod was heated in a water cooled mini e-beam evaporator. We choose a very low Mo flux that gave a deposition rate of $\sim 5 \times 10^{-4}$ ML per minute, where we define one monolayer (ML) as the number of Mo atoms in a single layer of MoTe2. For Ti deposition, a flux of $\sim 2 \times 10^{-4}$ ML per minute was measured. This low deposition rate allows for single Mo or Ti atoms to equilibrate with the surface before meeting other deposited metals at the surface. Deposition was carried out with the sample at RT or at elevated temperature of 350 °C.

STM Characterization. After deposition, the samples were transferred *in situ* from the preparation chamber into an analysis chamber for characterization by RT scanning tunneling microscopy (STM). The analysis chamber hosts an Omicron STM-1. Electrochemically etched W-tips are used for imaging. The MTB defects are more easily imaged under filled state conditions, and the detailed imaging conditions are reported in the STM figures. The contrast of the line defects is compared to simulated STM images to confirm the structure of the line defects.

ARPES Measurements. The analysis chamber also houses a hemispherical analyzer (Scienta R3000) with a 2D detector for angle-resolved photoemission spectroscopy (ARPES) measurements. A refocused helium discharge lamp providing nonpolarized He-I or He-II light is used for the excitation source. All spectra were acquired with the sample at RT.

Density Functional Theory. Density functional theory (DFT) calculations were carried out in the framework of projector-augmented waves as implemented in the VASP code. 35,36 We adopt the PBE exchange—correlation functional and account for spin-polarization throughout. The defective systems are modeled using 10 × 10

supercells, with the Brillouin zone sampled using solely the Γ -point. Migration barriers are evaluated with the help of the climbing image nudged elastic band approach. ³⁷

ASSOCIATED CONTENT

Supporting Information

The Supporting Information is available free of charge on the ACS Publications website at DOI: 10.1021/acsnano.8b01580.

Estimation of diffusion barriers calculated by DFT for lowest diffusion path ways. ARPES data of pristine and MTB modified MoTe₂ and MoSe₂ that show the change of the VBM at the K-point after formation of MTB networks (PDF)

AUTHOR INFORMATION

Corresponding Author

*E-mail: mbatzill@usf.edu.

ORCID ®

Hannu-Pekka Komsa: 0000-0002-0970-0957 Arkady V. Krasheninnikov: 0000-0003-0074-7588

Matthias Batzill: 0000-0001-8984-8427

Author Contributions

P.M.C., H.C.D., and Y.M. performed the STM and ARPES studies of MTB modified TMDs. H.-P. K. and A.V.K. performed DFT simulations. A.V.K and M.B. directed the research and wrote the paper.

Notes

The authors declare no competing financial interest.

ACKNOWLEDGMENTS

The authors acknowledge support from the National Science Foundation under award ECCS-1608654. We thank the Academy of Finland for the support under project nos. 286279 and 311058. We also thank CSC-IT Center for Science Ltd. and generous grants of computer time and PRACE for awarding us access to Hazel Hen at High Performance Computing Center, University of Stuttgart, Germany.

REFERENCES

- (1) Wei, X.; Wang, M.-S.; Bando, Y.; Golberg, D. Electron-Beam-Induced Substitutional Carbon Doping of Boron Nitride Nanosheets, Nanoribbons, and Nanotubes. *ACS Nano* **2011**, *5*, 2916–2922.
- (2) Wang, H.; Wang, Q.; Cheng, Y.; Li, K.; Yao, Y.; Zhang, Q.; Dong, C.; Wang, P.; Schwingenschlögl, U.; Yang, W.; Zhang, X. X. Doping Monolayer Graphene with Single Atom Substitutions. *Nano Lett.* **2012**, *12*, 141–144.
- (3) Lin, Y.-C.; Björkman, T.; Komsa, H.-P.; Teng, P.-Y.; Yeh, C.-H.; Huang, F.-S.; Lin, K.-H.; Jadczak, J.; Huang, Y.-S.; Chiu, P. W.; Krasheninnikov, A. V.; Suenaga, K. Three-Fold Rotational Defects in Two-Dimensional Transition Metal Dichalcogenides. *Nat. Commun.* **2015**, *6*, 6736.
- (4) Sutter, E.; Huang, Y.; Komsa, H.-P.; Ghorbani-Asl, M.; Krasheninnikov, A. V.; Sutter, P. Electron-Beam Induced Transformations of Layered Tin Dichalcogenides. *Nano Lett.* **2016**, *16*, 4410–4416.
- (5) Lin, Y.-C.; Dumcenco, D. O.; Huang, Y.-S.; Suenaga, K. Atomic Mechanism of the Semiconducting-to-Metallic Phase Transition in Single-layered MoS₂. *Nat. Nanotechnol.* **2014**, *9*, 391–396.
- (6) Kappera, R.; Voiry, D.; Yalcin, S. E.; Branch, B.; Gupta, G.; Mohite, A. D.; Chhowalla, M. Phase-Engineered Low-Resistance Contacts for Ultrathin MoS₂ Transistors. *Nat. Mater.* **2014**, *13*, 1128–1134
- (7) Wang, Y.; Xiao, J.; Zhu, H.; Li, Y.; Alsaid, Y.; Fong, K. Y.; Zhou, Y.; Wang, S.; Shi, W.; Wang, Y.; Zettl, A.; Reed, E. J.; Zhang, X.

Commun. 2015, 6, 8311.

Structural Phase Transition in Monolayer MoTe₂ Driven by Electrostatic Doping. *Nature* **2017**, *550*, 487–491.

- (8) Ma, Q.; Isarraraz, M.; Wang, C. S.; Preciado, E.; Klee, V.; Bobek, S.; Yamaguchi, K.; Li, E.; Odenthal, P. M.; Nguyen, A.; Barroso, D.; Sun, D.; von Son Palacio, G.; Gomez, M.; Nguyen, A.; Le, D.; Pawin, G.; Mann, J.; Heinz, T. F.; Rahman, T. S.; Bartels, L. Postgrowth Tuning of the Bandgap of Single-Layer Molybdenum Disulfide Films by Sulfur/Selenium Exchange. ACS Nano 2014, 8, 4672–4677.
- (9) Huang, C.; Wu, S.; Sanchez, A. M.; Peters, J. J. P.; Beanland, R.; Ross, J. S.; Rivera, P.; Yao, W.; Cobden, D. H.; Xu, X. Lateral Heterojunctions within Monolayer MoSe₂–WSe₂ Semiconductors. *Nat. Mater.* **2014**, *13*, 1096–1101.
- (10) Sutter, P.; Huang, Y.; Sutter, E. Nanoscale Integration of Two-Dimensional Materials by Lateral Heteroepitaxy. *Nano Lett.* **2014**, *14*, 4846–4851.
- (11) Lehtinen, O.; Komsa, H.-P.; Pulkin, A.; Whitwick, M. B.; Chen, M. W.; Lehnert, T.; Mohn, M. J.; Yazyev, O. V.; Kis, A.; Kaiser, U.; Krasheninnikov, A. V. Atomic Scale Microstructure and Properties of Se-Deficient Two-Dimensional MoSe₂. ACS Nano **2015**, *9*, 3274–3283
- (12) Lin, J.; Pantelides, S. T.; Zhou, W. Vacancy-Induced Formation and Growth of Inversion Domains in Transition-Metal Dichalcogenide Monolayer. *ACS Nano* **2015**, *9*, 5189–5197.
- (13) van der Zande, A. M.; Huang, P. H.; Chenet, D. A.; Berkelbach, T. C.; You, Y. M.; Lee, G.-H.; Heinz, T. F.; Reichman, D. R.; Muller, D. A.; Hone, J. C. Grains and Grain Boundaries in Highly Crystalline Monolayer Molybdenum Disulphide. *Nat. Mater.* **2013**, *12*, 554–561.
- (14) Ly, T. H.; Perello, D. J.; Zhao, J.; Deng, Q.; Kim, H.; Han, G. H.; Chae, S. H.; Jeong, H. Y.; Lee, Y. H. Misorientation-Angle-Dependent Electrical Transport Across Molybdenum Disulfide Grain Boundaries. *Nat. Commun.* **2016**, *7*, 10426.
- (15) Zhang, Z.; Zou, X.; Crespi, V. H.; Yakobson, B. I. Intrinsic Magnetism of Grain Boundaries in Two-Dimensional Metal Dichalcogenides. ACS Nano 2013, 7, 10475–10481.
- (16) Ma, Y.; Kolekar, S.; Coy Diaz, H.; Aprojanz, J.; Miccoli, I.; Tegenkamp, C.; Batzill, M. Metallic Twin Grain Boundaries Embedded in MoSe₂ Monolayers Grown by Molecular Beam Epitaxy. *ACS Nano* **2017**, *11*, 5130–5139.
- (17) Zhou, W.; Zou, X.; Najmaei, S.; Liu, Z.; Shi, Y.; Kong, J.; Lou, J.; Ajayan, P. M.; Yakobson, B. I.; Idrobo, J. C. Intrinsic Structural Defects in Monolayer Molybdenum Disulfide. *Nano Lett.* **2013**, *13*, 2615–2622.
- (18) Komsa, H.-P.; Krasheninnikov, A. V. Engineering the Electronic Properties of Two-Dimensional Transition Metal Dichalcogenides by Introducing Mirror Twin Boundaries. *Adv. Electr. Mater.* **2017**, *3*, 1600468.
- (19) Zhu, H.; Wang, Q.; Cheng, L.; Addou, R.; Kim, J.; Kim, M. J.; Wallace, R. M. Defects and Surface Structural Stability of MoTe₂ Under Vacuum Annealing. *ACS Nano* **2017**, *11*, 11005–11014.
- (20) Liu, L.; Jiao, L.; Yang, F.; Cai, Y.; Wu, X.; Ho, W.; Gao, C.; Jia, J.; Wang, N.; Fan, H.; Yao, W.; Xie, M. Dense Network of One-Dimensional Midgap Metallic Modes in Monolayer MoSe₂ and Their Spatial Undulations. *Phys. Rev. Lett.* **2014**, *113*, 066105.
- (21) Diaz, H. C.; Ma, Y.; Chaghi, R.; Batzill, M. High Density of (Pseudo) Periodic Twin-Grain Boundaries in Molecular Beam Epitaxy-Grown van der Waals Heterostructure: MoTe₂/MoS₂. *Appl. Phys. Lett.* **2016**, *108*, 191606.
- (22) Zou, X.; Liu, Y.; Yakobson, B. I. Predicting Dislocations and Grain Boundaries in Two-Dimensional Metal-Disulfides from First Principles. *Nano Lett.* **2013**, *13*, 253–258.
- (23) Ma, Y.; Diaz, H. C.; Avila, J.; Chen, C.; Kalappattil, V.; Das, R.; Phan, M.-H.; Cadez, T.; Carmelo, J. M. P.; Asensio, M. C.; Batzill, M. Angle Resolved Photoemission Spectroscopy Reveals Spin Charge Separation in Metallic MoSe₂ Grain Boundary. *Nat. Commun.* **2017**, *8*, 14231.
- (24) Barja, S.; Wickenburg, S.; Liu, Z.-F.; Zhang, Y.; Ryu, H.; Ugeda, M. M.; Hussain, Z.; Shen, Z.-X.; Mo, S.-K.; Wong, E.; Salmeron, M. B.; Wang, F.; Crommie, M. F.; Ogletree, D. F.; Neaton, J. B.; Weber-

Bargioni, A. Charge Density Wave Order in 1D Mirror Twin Boundaries of Single-Layer MoSe₂. Nat. Phys. **2016**, 12, 751.

- (25) Herbig, C.; Knispel, T.; Simon, S.; Schröder, U. A.; Martínez-Galera, A. J.; Arman, M. A.; Teichert, C.; Knudsen, J.; Krasheninnikov, A. V.; Michely, T. From Permeation to Cluster Arrays: Graphene on Ir(111) Exposed to Carbon Vapor. *Nano Lett.* **2017**, *17*, 3105–3112. (26) Chou, S. S.; Sai, N.; Lu, P.; Coker, E. N.; Liu, S.; Artyushkova, K.; Luk, T. S.; Kaehr, B.; Brinker, C. J. Understanding Catalysis in a Multiphasic Two-Dimensional Transition Metal Dichalcogenide. *Nat.*
- (27) Seok, J.; Lee, J.-H.; Cho, S.; Ji, B.; Kim, H. W.; Kwon, M.; Kim, D.; Kim, Y.-M.; Oh, S. H.; Kim, S. W.; Lee, Y. H.; Son, Y.-W.; Yang, H. Active Hydrogen Evolution Through Lattice Distortion in Metallic MoTe₂. 2D Mater. **2017**, *4*, 025061.
- (28) Sung, J. H.; Heo, H.; Si, S.; Kim, Y. H.; Noh, H. R.; Song, K.; Kim, J.; Lee, C.-S.; Seo, S.-Y.; Kim, D.-H.; Kim, H. K.; Yeom, H. W.; Kim, T.-H.; Choi, S.-Y.; Kim, J. S.; Jo, M.-H. Coplanar Semi-conductor—Metal Circuitry Defined on Few-Layer MoTe₂ via Polymorphic Heteroepitaxy. Nat. Nanotechnol. 2017, 12, 1064—1070.
- (29) Cho, S.; Kim, S.; Kim, J. H.; Zhao, J.; Seok, J.; Keum, D. H.; Baik, J.; Choe, D.-H.; Chang, J. J.; Suenaga, K.; Kim, S. W.; Lee, Y. H.; Yang, H. Phase Patterning for Ohmic Homojunction Contact in MoTe₂. *Science* **2015**, *349*, 625–628.
- (30) Qi, D.; Wang, Q.; Han, C.; Jiang, J.; Zheng, Y.; Chen, W.; Zhang, W.; Wee, A. T. S. Reducing the Schottky Barrier between Few-Layer MoTe, and Gold. 2D Mater. 2017, 4, 045016.
- (31) Diaz, H. C.; Chaghi, R.; Ma, Y.; Batzill, M. Molecular Beam Epitaxy of the van der Waals Heterostructure MoTe₂ on MoS₂: Phase, Thermal, and Chemical Stability. 2D Mater. 2015, 2, 044010.
- (32) Addou, R.; McDonnell, S.; Barrera, D.; Guo, Z. B.; Azcatl, A.; Wang, J.; Zhu, H.; Hinkle, C. L.; Quevedo-Lopez, M.; Alshareef, H. N.; Colombo, L.; Hsu, J. W. P.; Wallace, R. M. Impurities and Electronic Property Variations of Natural MoS₂ Crystal Surfaces. *ACS Nano* **2015**, *9*, 9124–9133.
- (33) Hong, J.; Wang, C.; Liu, H.; Ren, X.; Chen, J.; Wang, G.; Jia, J.; Xie, M.; Jin, C.; Ji, W.; Yuan, J.; Zhang, Z. Inversion Domain Boundary Induced Stacking and Bandstructure Diversity in Bilayer MoSe₂. *Nano Lett.* **2017**, *17*, 6653–6660.
- (34) Allain, A.; Kang, J.; Banerjee, K.; Kis, A. Electrical Contacts to Two-Dimensional Semiconductors. *Nat. Mater.* **2015**, *14*, 1195–1205. (35) Kresse, G.; Hafner, J. *Ab initio* Molecular Dynamics for Liquid
- Metals. *Phys. Rev. B: Condens. Matter Mater. Phys.* **1993**, *47*, 558–561. (36) Kresse, G.; Hafner, J. *Ab initio* Molecular-Dynamics Simulation of the Liquid-Metal—Amorphous-Semiconductor Transition in
- of the Liquid-Metal—Amorphous-Semiconductor Transition in Germanium. *Phys. Rev. B: Condens. Matter Mater. Phys.* **1994**, 49, 14251—14269.
- (37) Henkelman, G.; Uberuaga, B. P.; Jónsson, H. A Climbing Image Nudged Elastic Band Method for Finding Saddle Points and Minimum Energy Paths. *J. Chem. Phys.* **2000**, *113*, 9901–9904.